

Correlation of Gravitational Wave Background Noises and Statistical Loss for Angular Averaged Sensitivity Curves

Naoki Seto

Department of Physics, Kyoto University, Kyoto 606-8502, Japan

(Dated: August 31, 2021)

Gravitational wave backgrounds generate correlated noises to separated detectors. This correlation can induce statistical losses to actual detector networks, compared with idealized noise-independent networks. Assuming that the backgrounds are isotropic, we examine the statistical losses specifically for the angular averaged sensitivity curves, and derive simple expressions that depend on the overlap reduction functions and the strength of the background noises relative to the instrumental noises. For future triangular interferometers such as ET and LISA, we also discuss preferred network geometries to suppress the potential statistical losses.

I. INTRODUCTION

Gravitational wave astronomy has evolved rapidly after the detection of the first event GW150914 [1, 2]. The sensitivities of the current generation detectors have been improved gradually [3]. In addition, we have various future plans to observe gravitational waves at broad frequency regimes. For example, around 10-1000Hz, Einstein telescope (ET) [4] and Cosmic Explore [5] will have ~ 10 times better sensitivities than advanced LIGO. Furthermore, they will push the low-frequency noise walls down to ~ 1 Hz. In space, LISA [6, 7], TianQin [8, 9] and Taiji [10] are proposed to explore the mHz band, while B-DECIGO and DECIGO are targeting the 0.1Hz band [11].

The scientific prospects of these future projects have been widely discussed with various statistical quantities such as the parameter estimation errors for individual astrophysical sources and their detectable volumes (see e.g. [3]). Here, some of these quantities depend strongly on the geometries of the detector networks.

Stochastic gravitational wave backgrounds are interesting observational targets. For their detection, the correlation analysis is an effective approach, and enables us to detect a weak background whose strain spectrum is $\sim (fT_{\text{int}})^{-1/2}$ times smaller than the instrumental noise spectra (defined in units of Hz^{-1} not $\text{Hz}^{-1/2}$) [12–16]. Here f is the frequency of the background waves and T_{int} is the integration time for the correlation analysis.

Meanwhile, considering our limited understandings on high energy physics and early universe, we cannot securely impose tight upper limits on the magnitudes of backgrounds, purely from a theoretical standpoint. Indeed, there are variety of cosmological scenarios to generate backgrounds at various frequency regimes (see e.g. [17]). Therefore, in the new observational windows opened by the future projects, practically unconstrained by current observations, we might actually have a background comparable to the designed instrumental noises.

The angular averaged sensitivity is one of the basic measures to characterize gravitational wave detectors [7, 18]. If the noises of detectors are statistically independent and have an identical spectrum, the angu-

lar averaged sensitivity of their network should follow a simple scaling relation with respect to the number of detectors. But, in reality, gravitational wave backgrounds can induce correlated noises between separated detectors [12–14, 16]. Resultantly, the background noises break the simple scaling relation for the angular averaged sensitivity. The situation should depend on the geometry of the detector network and the strength of the background noises relative to the instrumental noises.

In this paper, we quantify the statistical losses due to the background noise correlation, by evaluating the deviation from the simple scaling relation. We also discuss preferred network geometries to suppress the statistical losses both for ground-based and space-borne detector networks.

This paper is organized as follows. In Sec. II, we study a basic model for two L-shaped detectors. In Sec. III, we discuss the networks composed by two triangular detectors tangential to a sphere. In Sec. IV, for future detectors, we numerically discuss the dependence of the statistical losses on the network geometry. Sec. V is devoted to summary and discussion.

II. ANGULAR AVERAGED SENSITIVITY

A. Noise Components

We consider an effectively L-shaped interferometer (with the label I) and decompose its data stream a_I in the Fourier space as

$$a_I(f) = h_I(f) + n_{ID}(f) + n_{IB}(f). \quad (1)$$

Here $h_I(f)$ represents a gravitational wave signal (e.g. from a compact binary), $n_{ID}(f)$ the instrumental noise and $n_{IB}(f)$ the noise due to isotropic gravitational wave backgrounds. The two noises are assumed to be stationary and Gaussian distributed. We define the instrumental noise spectrum $N_D(f)$ by

$$\langle n_{ID}(f)n_{ID}(f')^* \rangle = \delta(f - f')N_D(f) \quad (2)$$

with the ensemble average $\langle \dots \rangle$ and the delta function $\delta(\cdot)$. We also define the background noise spectrum

$N_B(f)$ by

$$\langle n_{IB}(f)n_{IB}(f')^* \rangle = \delta(f - f')N_B(f). \quad (3)$$

Hereafter, for notional simplicity, we omit the delta functions, using expressions for $f = f'$.

Similarly, we consider the second L-shaped interferometer II and represent its data stream by

$$a_{II}(f) = h_{II}(f) + n_{IID}(f) + n_{IIB}(f). \quad (4)$$

We assume that its instrumental noise spectrum is identical to the first one I as

$$\langle n_{IID}(f)n_{IID}(f)^* \rangle = N_D(f), \quad (5)$$

but is statistically independent as $\langle n_{ID}(f)n_{IID}(f)^* \rangle = 0$. Actually, a weak correlation of instrumental noises does not largely change the present study. This is different from the requirement at detecting a weak gravitational wave background by the correlation analysis (see e.g. [19–21]).

For the background noise of the second interferometer II, we put

$$\langle n_{IIB}(f)n_{IIB}(f)^* \rangle = N_B(f). \quad (6)$$

We should notice that, in contrast to the instrumental noises, the background noises would have a definite correlation

$$\langle n_{IB}(f)n_{IIB}(f)^* \rangle = N_B(f)\gamma(f) \quad (7)$$

characterized by the overlap reduction function (ORF) $\gamma(f)$ with $-1 \leq \gamma(f) \leq 1$ (see e.g. [12–14, 22]).

Then, the noise matrix can be expanded as ($i, j = \text{I, II}$)

$$\begin{aligned} N_{ij}(f) &\equiv \langle \{n_{iD}(f) + n_{iB}(f)\}^* \{n_{jD}(f) + n_{jB}(f)\} \rangle \\ &= (N_D(f) + N_B(f)) \begin{pmatrix} 1 & \frac{K\gamma}{(1+K)} \\ \frac{K\gamma}{(1+K)} & 1 \end{pmatrix}. \end{aligned} \quad (8)$$

Here we defined the ratio between the two noise components by

$$K(f) \equiv \frac{N_B(f)}{N_D(f)}. \quad (9)$$

The two parameters γ and K play important roles in the analysis below.

B. Averaged Signal-to-Noise Ratio

Next, we discuss the angular averaged sensitivities of detector networks to gravitational wave signals. To begin with, we examine the signal analysis with the single interferometer I, and put its gravitational wave signal $h_I(f, \alpha)$. Here we introduced the parameter α to abstractly show the polarization and direction angles. As in the case of

evaluating the angular averaged sensitivity curve, we take the following ratio as an intermediate product [23]

$$\sigma_1 = \frac{\langle h_I(f, \alpha)h_I(f, \alpha)^* \rangle_\alpha}{N_D(f) + N_B(f)}, \quad (10)$$

where $\langle \dots \rangle_\alpha$ represents the averages with respect to the polarization and direction angles. Roughly speaking, the square root of σ_1 is proportional to the signal strength relative to the noise around the frequency f . Since we will soon compare σ_1 with $\sigma_{\mathcal{N}}$ defined for multiple detectors, the common factors were dropped in Eq. (10).

For a network composed by totally \mathcal{N} detectors of the identical specifications, we can extend Eq. (10) in the matrix form as [23]

$$\sigma_{\mathcal{N}} = \sum_{ij}^{\mathcal{N}} \langle h_i(f, \alpha)h_j(f, \alpha)^* \rangle_\alpha N_{ij}(f)^{-1}. \quad (11)$$

Then we use the ratio $\sigma_{\mathcal{N}}/\sigma_1$ to measure the statistical gain of the angular averaged sensitivity by using \mathcal{N} detectors, compared with the single one. For a network with noise independent equivalent detectors, we readily obtain $\sigma_{\mathcal{N}}/\sigma_1 = \mathcal{N}$. On the other hand, if we have correlated background noises, the effective number of detectors could be smaller than \mathcal{N} .

Next, we specifically examine the case $\mathcal{N} = 2$. For the signal matrix $\langle h_i(f, \alpha)h_j(f, \alpha) \rangle_\alpha$ (with $i, j = \text{I, II}$), the diagonal elements have the relation

$$\langle h_I(f, \alpha)h_I(f, \alpha)^* \rangle_\alpha = \langle h_{II}(f, \alpha)h_{II}(f, \alpha)^* \rangle_\alpha. \quad (12)$$

The off-diagonal elements can be expressed as [12–15]

$$\begin{aligned} \langle h_I(f, \alpha)h_{II}(f, \alpha)^* \rangle_\alpha &= \langle h_{II}(f, \alpha)h_I(f, \alpha)^* \rangle_\alpha \\ &= \gamma(f) \langle h_I(f, \alpha)h_I(f, \alpha)^* \rangle_\alpha \end{aligned} \quad (13)$$

with the ORF γ already used in Eq. (7).

Now, we evaluate the statistical gain σ_2/σ_1 . As mentioned earlier, this shows the improvement of the angular averaged sensitivity by using the two detectors. Appropriately cancelling common factors, we have

$$\frac{\sigma_2}{\sigma_1} = \text{Tr} \left[\begin{pmatrix} 1 & \gamma \\ \gamma & 1 \end{pmatrix} \begin{pmatrix} 1 & \frac{K\gamma}{(1+K)} \\ \frac{K\gamma}{(1+K)} & 1 \end{pmatrix}^{-1} \right] \quad (15)$$

$$= \frac{2(1+K)(1+K-\gamma^2K)}{(1+K)^2 - K^2\gamma^2} \quad (16)$$

$$\equiv G_2(K, \gamma). \quad (17)$$

In Fig. 1, we present a contour plot for the analytic expression $G_2(K, \gamma)$ which is an even function of γ .

We can easily confirm that the maximum value of G_2 is realized at $K = 0$ or $\gamma = 0$ as

$$G_2(0, \gamma) = G_2(K, 0) = 2. \quad (18)$$

For these sets of parameters (γ, K) , the noise matrix (8) becomes diagonal and the two detectors are statistically

independent. We thus obtain $G_2 = 2$, as easily expected. The deficit $2 - G_2(K, \gamma)$ shows the statistical loss induced by the background noise correlation.

For $K \ll 1$, we can expand $G_2(K, \gamma)$ as

$$G_2(K, \gamma) = 2(1 - K\gamma^2) + O(K^2). \quad (19)$$

In the limit $K \rightarrow \infty$, we have

$$\lim_{K \rightarrow \infty} G_2(K, \gamma) = 2 \quad (20)$$

for $\gamma \neq \pm 1$. In contrast, we obtain

$$\lim_{K \rightarrow \infty} G_2(K, \gamma = \pm 1) = 1. \quad (21)$$

Therefore, we have the inequality

$$\lim_{\gamma \rightarrow \pm 1} [\lim_{K \rightarrow \infty} G_2(K, \gamma)] \neq \lim_{K \rightarrow \infty} [\lim_{\gamma \rightarrow \pm 1} G_2(K, \gamma)], \quad (22)$$

showing the dependence on the order of the limiting operations.

At first sight, Eq. (20) might look counterintuitive. For example, let us consider two highly correlated detectors with $\gamma = 0.999$. They have the nearly the same signals

$$h_{\text{I}}(f, \alpha) \sim h_{\text{II}}(f, \alpha) \quad (23)$$

and, at $K \gg 1$, their noises also satisfy

$$n_{\text{ID}}(f) + n_{\text{IB}}(f) \sim n_{\text{IID}}(f) + n_{\text{IIB}}(f) \quad (24)$$

with the relation $n_{\text{IB}}(f) \sim n_{\text{IIB}}(f)$ for $\gamma \sim 1$. But this does not result in $G_2 \sim 1$. In fact, we can diagonalize the noise matrix (8) by taking the linear combination of the original data streams as

$$a' = \frac{(a_{\text{I}} - a_{\text{II}})}{\sqrt{2}}, \quad a'' = \frac{(a_{\text{I}} + a_{\text{II}})}{\sqrt{2}}. \quad (25)$$

At $K \rightarrow \infty$, the differential mode a' simultaneously reduces the largely overlapped background noises and the gravitational wave signals. More specifically, the noise spectrum of the differential mode a' is given by

$$N_D + N_B(1 - \gamma) \quad (26)$$

and the signal strength by

$$\langle h_{\text{I}}(f, \alpha) h_{\text{I}}(f, \alpha)^* \rangle_{\alpha} (1 - \gamma). \quad (27)$$

Meanwhile the total mode a'' has the noise spectrum

$$N_D + N_B(1 + \gamma) \quad (28)$$

and the signal

$$\langle h_{\text{I}}(f, \alpha) h_{\text{I}}(f, \alpha)^* \rangle_{\alpha} (1 + \gamma). \quad (29)$$

Thus, even for $\gamma \sim 1$ (but $\gamma \neq 1$), the signal-to-noise ratio of the differential mode a' is comparable to the total

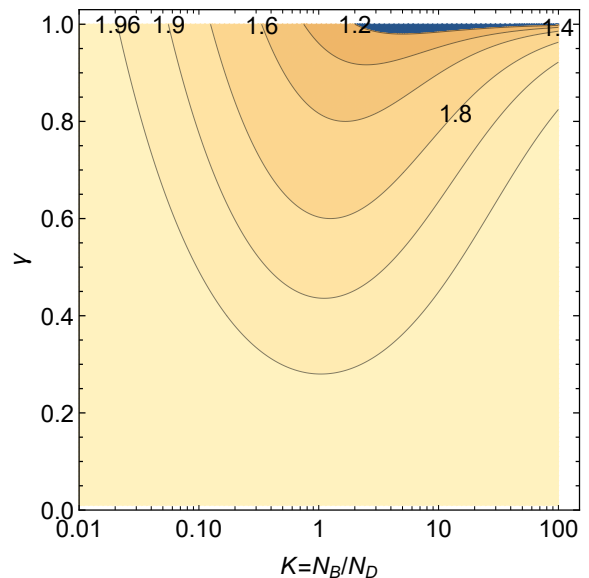


FIG. 1: Contour plot for the effective detector number $G_2(K, \gamma)$ defined for two L-shaped interferometers with the same instrumental noise spectrum. Their background noises have correlation, characterized by the ORF γ . The parameter K represents the ratio between the background and instrumental noises. We have $1 \leq G_2(K, \gamma) \leq 2$ with $G_2(0, \gamma) = G_2(K, 0) = 2$.

mode a'' at $K = N_B/N_D \rightarrow \infty$. In contrast, at $K \sim (1 - \gamma)^{-1}$, this comparability is destroyed by the incoherent instrumental noise contribution $N_D(f)$ in Eq. (26).

For a newly opened frequency window of gravitational waves, the ratio K cannot be securely predicted ahead of time. In principle, we can make theoretical estimations based on some models, or use cosmological constraints on primordial waves (see e.g. [24]). But it would be fruitful to extract insights that are independent of the ratio K . To this end, we evaluate the minimum value of $G_2(K, \gamma)$ for a given γ , as the worst case. By solving the equation $\partial_K G_2 = 0$ for K , we find the solution $K_{\min}(\gamma) = (1 - \gamma^2)^{-1/2}$ and obtain the corresponding minimum $G_2[K_{\min}(\gamma), \gamma] = 1 + \sqrt{1 - \gamma^2} \equiv G_{2\min}(\gamma)$ with

$$G_2(K, \gamma) \geq G_{2\min}(\gamma). \quad (30)$$

For the number of detectors $\mathcal{N} > 2$, Eq. (20) is generalized to $\lim_{K \rightarrow \infty} \sigma_{\mathcal{N}}/\sigma_1 = \mathcal{N}$, if none of the overlap reduction functions are 1 or -1 . This is because the instrumental noises can be ignored and Eq. (15) becomes the trace of the \mathcal{N} -dimensional unit matrix.

III. TWO TRIANGULAR DETECTORS ON A SPHERE

The ground based detector ET [4] and the space-borne detector LISA [7] are both planned to have triangular ge-

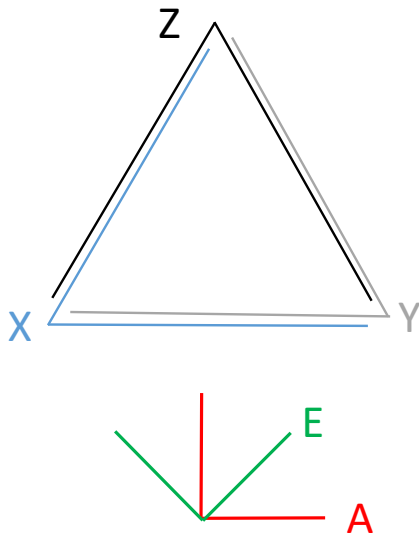


FIG. 2: The orientations of the two effective interferometers A and E made from the symmetric data streams X, Y and Z . The instrumental noises of A and E have no correlation, and their ORF is $\gamma_{AE} = 0$.

ometry. Such detectors have preferable symmetric structure and enable us to simplify otherwise cumbersome calculations. Therefore, below, we focus on networks composed by two equivalent triangular units. We should mention that the geometrical arguments in this section share similarities with Ref. [25, 26] done for a largely different topic (polarization modes of gravitational wave backgrounds).

A. Data Streams From a Single Triangular Unit

First, we briefly discuss the internal symmetry of a triangular unit. We assume that we can make three effective interferometers X, Y and Z symmetrically at each vertex, as shown in Fig. 2.

Next, we study the 3×3 matrix for their instrumental noises (n_X, n_Y, n_Z), omitting the apparent frequency dependence, for notational simplicity. Given the symmetry of the system, we can put

$$\langle n_X n_X^* \rangle = \langle n_Y n_Y^* \rangle = \langle n_Z n_Z^* \rangle = N_d \quad (31)$$

for the diagonal elements of the instrumental noise matrix. For the six off-diagonal elements, considering the symmetry and the potential correlations (e.g. due to the seismic noises for ET), we put

$$\langle n_X n_Y^* \rangle = \langle n_Y n_X^* \rangle = \langle n_X n_Z^* \rangle = \dots = N_o. \quad (32)$$

Therefore, the instrumental noises matrix becomes symmetric and can be diagonalized with an orthogonal matrix. For example, we take the three data combinations

[27, 28]

$$A = \frac{X - Y}{\sqrt{2}}, \quad E = \frac{X + Y - 2Z}{\sqrt{6}}, \quad (33)$$

$$T = \frac{X + Y + Z}{\sqrt{3}}. \quad (34)$$

Their instrumental noise matrix has the following diagonal components

$$N_{AA} = N_{EE} = N_d - N_o, \quad (35)$$

$$N_{TT} = N_d + 2N_o \quad (36)$$

with the off-diagonal ones $N_{AE} = N_{ET} = N_{TA} = \dots = 0$. Similarly using the underlying symmetry, we can also confirm the following relations for the ORFs

$$\gamma_{AE} = \gamma_{ET} = \gamma_{TA} = 0. \quad (37)$$

The information content is the same for (X, Y, Z) and (A, E, T) . But the latter would be more advantageous for the present study, exploiting the symmetries of the system (including the case with $N_o(f) = 0$).

In the next section, we discuss the statistical loss induced by the background noise correlation for two triangular units. Such effect is more important in the lower frequency regime. But, there, the sensitivity of the T -mode is much worse than the A and E modes, due to a signal cancellation. We can easily confirm this cancellation by applying the low frequency approximation to the original data (X, Y, Z) and then evaluating Eqs. (33) and (34). Below, we only keep the A and E modes that can be regarded as the two L-shaped interferometers whose orientations are shown in Fig. 2. In the connection to the previous section, we can put $N_D = N_d - N_o$ for their instrumental noise spectrum.

In fact, as shown in Eq. (35), the eigen values for the noise matrix are degenerated for the A and E modes, and we have the freedom to additionally introduce an orthogonal matrix and generate the new data combination [25]

$$A(\phi) = A \cos 2\phi + E \sin 2\phi, \quad (38)$$

$$E(\phi) = -A \sin 2\phi + E \cos 2\phi, \quad (39)$$

keeping Eqs. (35) and (37) invariant. As shown in the bottom panel of Fig. 2, this arrangement corresponds to virtually rotating the two interferometers A and E counterclockwise by the angle ϕ . The factor of 2 is due to the spin-2 nature of the detector tensor.

B. Two Triangular Units on a Sphere

Next, we discuss two triangular units U_1 and U_2 that have identical specifications and are tangential to a sphere with radius R . We put (A, E) for the data streams of U_1 and (A', E') for U_2 . Our primary objective in this

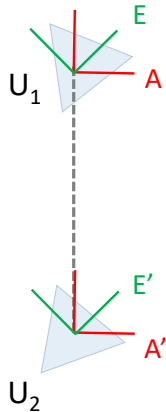


FIG. 3: Adjusted orientations of the effectively L-shaped interferometers A, E, A' and E' . These four are generated from the two triangular detectors U_1 and U_2 tangential to a sphere. The dashed line shows the geodesic (great circle) connecting the two triangle on the sphere. The effective interferometers A and A' have arms parallel or perpendicular to the geodesic, and E and E' are misaligned by 45° . Due to the geometrical symmetry, we have the ORFs $\gamma_{AE} = \gamma_{A'E'} = \gamma_{AE'} = \gamma_{A'E} = 0$.

subsection is to evaluate effective gain σ_{2U}/σ_{1U} by using the two units $U_1 + U_2$ compared with the single unit U_1 .

Since we have the four effective interferometers (A, E, A', E') , the matrices in Eq. (11) would be 4×4 . However, applying a simple trick associated with Eqs. (38) and (39), we can largely simplify the problem. As pointed out in [25, 26], by using the freedom of the virtual rotation, we can align the orientations of the effective interferometers (A, E, A', E') , following the great circle connecting the two units on the contact sphere (see Fig. 3). Below, we use the notations (A, E, A', E') to represent the interferometers after the adjustments.

Using the reflection symmetry of the system, we can show

$$\gamma_{AE'} = \gamma_{EA'} = 0 \quad (40)$$

along with $\gamma_{AE} = \gamma_{A'E'} = 0$ (see Eq. (37)) [25]. Then, the 4×4 matrices are block diagonalized for the pairs (A, A') and (E, E') . Accordingly, the effective number of the triangular units σ_{2U}/σ_{1U} can be simply expressed by

$$G_\Delta(K, \gamma_{AA'}, \gamma_{EE'}) = \frac{1}{2} \{G_2(K, \gamma_{AA'}) + G_2(K, \gamma_{EE'})\} \quad (41)$$

A single triangular unit provided the two independent interferometers A and E with $\gamma_{AE} = 0$. We thus have $\sigma_{1U}/\sigma_1 = 2$ with σ_1 defined for the A (or E) interferometer alone. Then we have $\sigma_{2U}/\sigma_{1U} = \sigma_1/\sigma_{1U} \cdot \sigma_{2U}/\sigma_1$ as in Eq. (41).

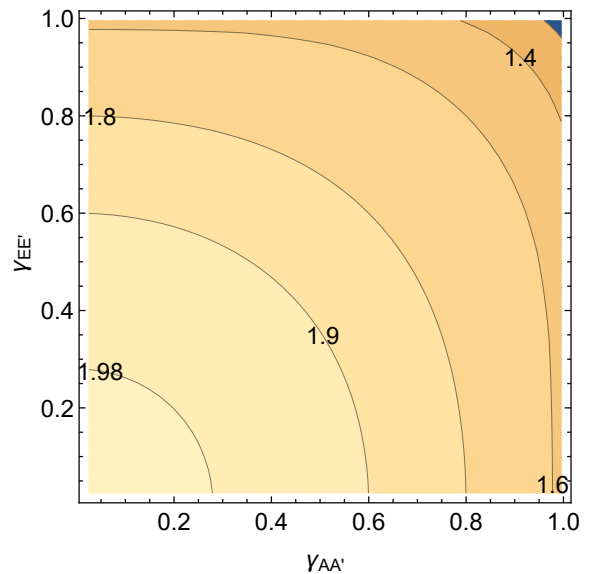


FIG. 4: Contour plot for the minimum value $G_{\Delta \min}(\gamma_{AA'}, \gamma_{EE'})$ of the statistical gain showing the effective number of triangular units. This function is symmetric with respect to the two arguments $\gamma_{AA'}$ and $\gamma_{EE'}$. We have $G_{\Delta \min}(0, 0) = 2$ and $G_{\Delta \min}(1, 1) = 1$.

From Eq. (16), the expression (41) does not depend on the signs of $\gamma_{AA'}$ and $\gamma_{EE'}$. Note that our method based on the symmetry cannot be applied to networks with more than two triangular units. From Sec. III, the maximum value of the statistical gain is $G_\Delta = 2$ (e.g. at $K = 0$). Thus, the statistical loss induced by the background noise correlation is estimated to be $2 - G_\Delta$.

For $K \ll 1$, from Eq. (19), we have

$$G_\Delta(K, \gamma_{AA'}, \gamma_{EE'}) = 2 - K(\gamma_{AA'}^2 + \gamma_{EE'}^2) + O(K^2) \quad (42)$$

This expression might be useful for a weak background noise. Given $|\gamma_{AA'}| \leq 1$ and $|\gamma_{EE'}| \leq 1$, the loss can be at most $\sim 2K$ for $K \ll 1$.

C. Minimum Values

As the worst case similar to Eq. (30), we can evaluate the minimum value $G_{\Delta \min}(\gamma_{AA'}, \gamma_{EE'})$ of the function $G_\Delta(K, \gamma_{AA'}, \gamma_{EE'})$ by changing K for given $\gamma_{AA'}$ and $\gamma_{EE'}$. The corresponding point $K = K_{\min}(\gamma_{AA'}, \gamma_{EE'})$ is given as a solution of a hexic polynomial equation $\partial_K G_\Delta = 0$ whose coefficients are given by $\gamma_{AA'}$ and $\gamma_{EE'}$. Then we can formally express the minimum value by

$$G_{\Delta \min}(\gamma_{AA'}, \gamma_{EE'}) \equiv G_\Delta[K_{\min}(\gamma_{AA'}, \gamma_{EE'}), \gamma_{AA'}, \gamma_{EE'}]. \quad (43)$$

On the other hand, by applying inequality (30) individually to the two terms in the right hand side of Eq.

(41), we can also obtain a weaker bound as

$$G_{\Delta \min}^{\dagger}(\gamma_{AA'}, \gamma_{EE'}) \equiv \frac{1}{2} [G_{2 \min}(\gamma_{AA'}) + G_{2 \min}(\gamma_{EE'})] \quad (44)$$

with the function $G_{2 \min}(x) \equiv 1 + \sqrt{1 - x^2}$ defined for Eq. (30). The two functions $G_{\Delta \min}$ and $G_{\Delta \min}^{\dagger}$ are symmetric with respect to the arguments $(\gamma_{AA'}, \gamma_{EE'})$. From their definitions, we have

$$\begin{aligned} G_{\Delta}(K, \gamma_{AA'}, \gamma_{EE'}) &\geq G_{\Delta \min}(\gamma_{AA'}, \gamma_{EE'}) \\ &\geq G_{\Delta \min}^{\dagger}(\gamma_{AA'}, \gamma_{EE'}). \end{aligned} \quad (45)$$

In fact, the simple function $G_{\Delta \min}^{\dagger}$ is a good approximation to the complicated one $G_{\Delta \min}$. We numerically examined the difference

$$G_{\Delta \min}(\gamma_{AA'}, \gamma_{EE'}) - G_{\Delta \min}^{\dagger}(\gamma_{AA'}, \gamma_{EE'}) \quad (46)$$

in the two dimensional region $0 \leq \gamma_{AA'} \leq \gamma_{EE'} \leq 1$. It exactly vanishes on the two boundaries: $\gamma_{AA'} = \gamma_{EE'}$ and $\gamma_{AA'} = 0$. The maximum value of the difference is ~ 0.08 around $(\gamma_{AA'}, \gamma_{EE'}) = (0.7, 1)$. But the difference is less than 0.01 for the slightly restricted region

$$0 \leq \gamma_{AA'} \leq \gamma_{EE'} \leq 0.93. \quad (47)$$

Below, we numerically handle the full expression $G_{\Delta \min}$ without using its approximation $G_{\Delta \min}^{\dagger}$.

D. Numerical Results

Next we concretely evaluate the two ORFs $\gamma_{AA'}$ and $\gamma_{EE'}$ for the aligned configuration (as in Fig. 3) on a sphere with radius R . The spatial distance between the two units are given by $D = 2R \sin(\beta/2)$ with the opening angle β ($0^\circ \leq \beta \leq 180^\circ$) measured from the center of the contact sphere. We define the characteristic frequency $f_R \equiv c/(2\pi R)$, and introduce the rescaled one as

$$\eta \equiv \frac{f}{f_R}. \quad (48)$$

Then, the two ORFs are expressed as [25]

$$\gamma_{AA'}(\eta, \beta) = \Theta_1(y, \beta) - \Theta_2(y, \beta) \quad (49)$$

$$\gamma_{EE'}(\eta, \beta) = \Theta_1(y, \beta) + \Theta_2(y, \beta) \quad (50)$$

with the variable

$$y \equiv \frac{2\pi f D}{c} = 2 \sin\left(\frac{\beta}{2}\right) \eta. \quad (51)$$

The functions $\Theta_{1,2}$ are given by the spherical Bessel func-

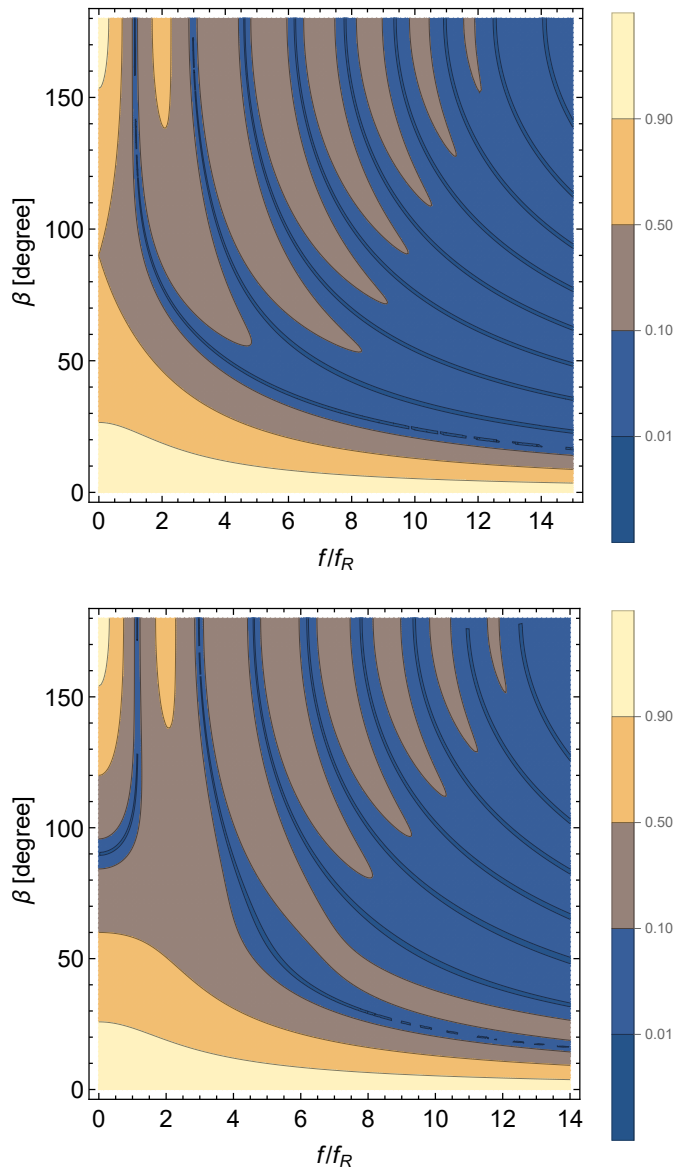


FIG. 5: Contour plots for the ORFs $|\gamma_{AA'}|$ (upper) and $|\gamma_{EE'}|$ (lower). The interferometers (A, E, A', E') are virtually aligned by using the geodesic as in Fig. 3. The parameter β represents their angular separation measured from the center of the contact sphere. We use the scaled frequency $\eta = f/f_R$ with $f_R \equiv c/(2\pi R)$.

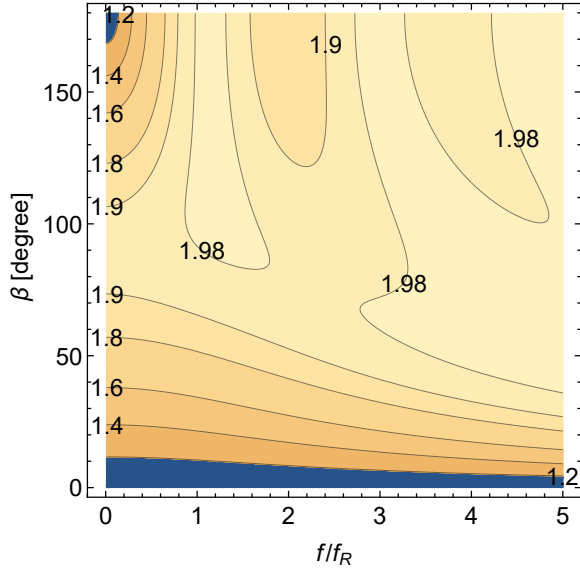


FIG. 6: Contour plot for the lower bound $G_{\Delta \min}(\gamma_{AA'}, \gamma_{EE'})$ defined in Eq. (43). We have $f_R = 7.58\text{Hz}$ for ground based detectors and $f_R = 0.28\text{mHz}$ for LISA-like detectors.

tions as

$$\Theta_1(y, \beta) = \left(j_0(y) + \frac{5}{7}j_2(y) + \frac{3}{112}j_4(y) \right) \cos^4\left(\frac{\beta}{2}\right) \quad (52)$$

$$\begin{aligned} \Theta_2(y, \beta) = & \left(-\frac{3}{8}j_0(y) + \frac{45}{56}j_2(y) - \frac{169}{896}j_4(y) \right) \\ & + \left(\frac{1}{2}j_0(y) - \frac{5}{7}j_2(y) - \frac{27}{224}j_4(y) \right) \cos \beta \\ & + \left(-\frac{1}{8}j_0(y) - \frac{5}{56}j_2(y) - \frac{3}{896}j_4(y) \right) \cos 2\beta. \end{aligned} \quad (53)$$

In Fig. 5, we present the contour plots for $|\gamma_{AA'}|$ and $|\gamma_{EE'}|$. The dark blue lines roughly show the zero points of these functions.

Roughly speaking, because of the stronger phase coherence, the magnitudes of the ORFs become larger at lower frequency regime. In concrete terms, we have $\lim_{y \rightarrow 0} j_n(y) = \delta_{n0}$ and the corresponding asymptotic profiles

$$\gamma_{AA'}(0, \beta) = \frac{3 + \cos(2\beta)}{4}, \quad \gamma_{EE'}(0, \beta) = \cos(\beta). \quad (54)$$

The absolute values of these expressions are minimum both at $\beta = 90^\circ$. In Fig. 5, we also have $\gamma_{AA'} \rightarrow 1$ and $\gamma_{EE'} \rightarrow 1$ in the small angle limit $\beta \rightarrow 0$ (resulting in $y \rightarrow 0$ from Eq. (51)).

Given the ORFs, we can numerically evaluate the minimum value $G_{\Delta \min}$ for the statistical gain. In the next section, we discuss the preferred geometrical configuration for two units both on the Earth and in space. As a preparation, we provide the bound $G_{\Delta \min}$ as a function

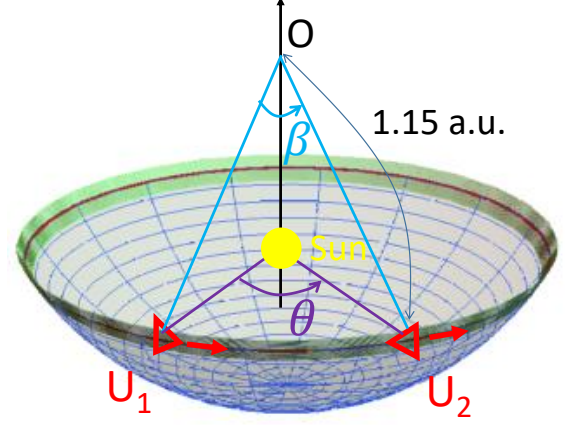


FIG. 7: Geometrical configuration of two LISA-like triangular units U_1 and U_2 . The two units move nearly on the ecliptic plane at the distance of ~ 1 a.u. from the Sun with the phase difference θ . The detector planes are inclined to the orbital (ecliptic) plane by 60° . Their envelope (green belt) are tangential to a virtual sphere of radius $R = 1.15$ a.u.. From the center O of the virtual sphere, the two units are separated by the angle β . The relation between θ and β is given in Eq. (57).

of the scaled frequency η and the separation angle β

$$G_{\Delta \min}(\eta, \beta) = G_{\Delta \min}[(\gamma_{AA'}(\eta, \beta), \gamma_{EE'}(\eta, \beta))]. \quad (55)$$

In Fig. 6, we present its contour plot. We can observe significant potential reduction of the gain $G_{\Delta \min} \lesssim 1.2$ at $\beta \lesssim 10^\circ$, reflecting the strong correlation $\gamma_{AA'} \sim \gamma_{EE'} \sim 1$ shown in Fig. 5. We also have the regime with $G_{\Delta \min} \lesssim 1.2$ at the upper left in this figure. Actually, at $(\eta, \beta) = (0, 180^\circ)$, we exactly obtain $G_{\Delta \min} = 1$ with $\gamma_{AA'} = 1$ and $\gamma_{EE'} = -1$.

In Fig. 6, on the vertical line $\eta = 0$, we have the peak value at $\beta = 90^\circ$

$$G_{\Delta \min}(\eta = 0, \beta = 90^\circ) = \frac{6 + \sqrt{3}}{4} \simeq 1.933 \quad (56)$$

directly from Eq. (54).

IV. APPLICATION FOR FUTURE PROJECTS

In this section, using Fig. 6, we discuss the statistical gains for networks composed by future triangular detectors.

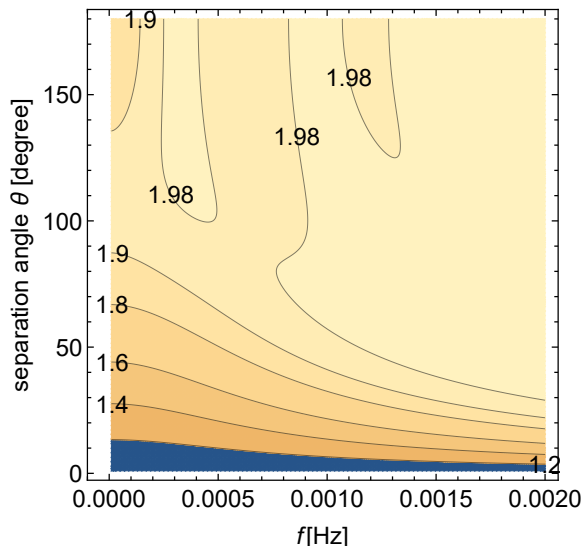


FIG. 8: Contour plot of the lower bound $G_{\Delta \min}(\gamma_{AA'}, \gamma_{EE'})$ for two LISA-like triangular units. In contrast to Fig. 6, the vertical axis is the orbital phase difference θ , instead of β (see Fig. 7) The proposed LISA-Taiji network has $\theta = 40^\circ$.

A. Ground-Based Detectors

First, we study two triangular detectors on the Earth, similar to ET. The Earth has the characteristic frequency $f_R = 7.58\text{Hz}$ for its radius $R = 6300\text{km}$. The scaled frequency is given by $\eta = (f/7.58\text{Hz})$.

At the low frequency regime, advanced LIGO (including its +version) and advanced Virgo will have steep noise walls around 10Hz ($\eta \sim 1.3$). One of the major improvements of ET is to push down the noise wall down to $\sim 1\text{Hz}$ ($\eta \sim 0.13$) and open the new window at $\eta = 0.1 \sim 1$ [4].

As an example, let us assume that we have two triangular units separated by $\beta \sim 27^\circ$ (corresponding to the Hanford-Livingston distance). Fig. 6 shows that the statistical gain could be as small as $G_{\Delta} \sim 1.5$ in the new window $\eta = 0.1 \sim 1$. To guarantee a large statistical gain $G_{\Delta} \gtrsim 1.9$ (i.e. a small statistical loss $2 - G_{\Delta}$) in the frequency range, we need to set the separation in the range $70^\circ \lesssim \beta \lesssim 110^\circ$.

B. LISA-Taiji Network

LISA is composed by three spacecrafts, approximately forming a regular triangular configuration. It rotates around the Sun nearly on the ecliptic plane with the semi-major axis 1 a.u.. As shown in Fig. 7 with the green belt, the envelope of the detector plane is inclined to the ecliptic plane by $\sim 60^\circ$. We consider two LISA-like units that share the envelope of the detector plane, separated by the angle θ corresponding to the orbital phase difference. For example, LISA and Taiji are planned to have

the phase difference $\theta = 40^\circ$ [25, 26, 29] (see also [30–33] for other configurations).

In fact, the envelope of the detector planes are tangential to a virtual sphere of radius $R = 2/\sqrt{3} = 1.15$ a.u.. The center O of the sphere is $1/\sqrt{3}$ a.u. away from the Sun. For the two units, the opening angle β from the center O is written with the phase difference θ as [25]

$$\beta = \arccos \left[\frac{(1 + 3 \cos \theta)}{4} \right] \equiv \beta(\theta). \quad (57)$$

For example, we have correspondences $(\theta, \beta) = (0^\circ, 0^\circ), (40^\circ, 35.1^\circ), (109.4^\circ, 90^\circ)$ and $(180^\circ, 120^\circ)$.

Now, we can apply Fig. 6 for two LISA-like units. For the virtual sphere with $R = 1.15$ a.u., the characteristic frequency is $f_R = 0.28\text{mHz}$ with the scaled one $\eta = (f/0.28\text{mHz})$. In Fig. 8, we show the contour plot generated from Fig. 6. This figure shows that, with the current design $\theta = 40^\circ$ for the LISA-Taiji network, we might have a relatively small gain $G_{\Delta} \sim 1.6$ at $f \lesssim 0.5\text{mHz}$ ($\eta \lesssim 1.8$). To realize $G_{\Delta} > 1.9$ at the whole frequency regime, we need to take the orbital phase difference at $89^\circ < \theta < 153^\circ$ (corresponding to $75^\circ < \beta < 105^\circ$). At the low frequency regime, the optimal choice is $\theta = 109.4^\circ$ ($\beta = 90^\circ$).

C. Galactic Confusion Noise

Next, we discuss the reduction of the statistical gain caused by the Galactic confusion noise made from unresolved Galactic binaries in the LISA band. In Fig. 9, we present the instrumental noise $N_D(f)$ of LISA and the estimated Galactic confusion noise spectrum $N_B(f)$ [18].

In reality, the Galactic confusion background is anisotropic (see e.g. [34–38]). Since the orientations of the triangle units change with time, their confusion noise spectra will be time dependent. Therefore, the spectrum $N_B(f)$ in Fig. 9 should be regarded as a time-averaged one.

In principle, we can develop a formulation for evaluating the statistical gain (as an extension of Secs. II and III) including the anisotropies of the Galactic background. However, we can no longer use the geometrical symmetries associated with isotropic backgrounds, and the intermediate calculations become much more complicated. For example, we cannot make the 2×2 block diagonalization with the alignment based on the geodesic (see Fig. 3). Furthermore, some of the correlation coefficients (e.g. $\gamma_{AA'}$) would be complex numbers, due to the odd multipoles of the incoming background waves.

Here, ignoring the anisotropies, we simply apply our expression $G_{\Delta}(K, \gamma_{AA'}, \gamma_{EE'})$ in Eq. (32) for approximately evaluating the statistical gain affected by the Galactic confusion noise. We use the ORFs $\gamma_{AA'}$ and $\gamma_{EE'}$ defined for isotropic backgrounds and also plug in the time averaged ratio $K(f) = N_B(f)/N_D(f)$ shown in Fig. 9.

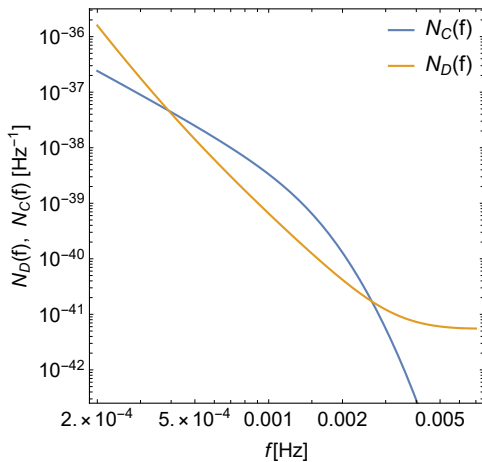


FIG. 9: The detector noise spectrum $N_D(f)$ of LISA and the estimated Galactic confusion noise spectrum $N_C(f)$ after 4yr integration [18]. These spectra are presented for the single L-shaped interferometers (corresponding to the A or E modes) without the angular averaging. The relative noise strength is given by $K(f) = N_C(f)/N_D(f)$.

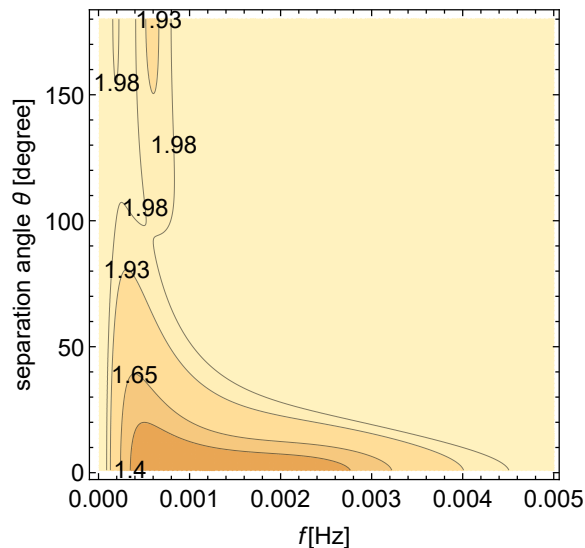


FIG. 10: The statistical gain $G_\Delta(K(f), \gamma_{AA'}(f), \gamma_{EE'}(f))$ for two LISA-like units. The vertical axis represents the orbital phase difference θ .

For an anisotropic background, the degree of the noise correlation (corresponding to the ORFs for an isotropic case) depends on the overall orientation of the network. Therefore, it will not be straightforward to tell whether the present approximation overestimates or underestimates the actual statistical gain.

We expect that our simplified treatment would be a convenient approximation, roughly taking into account the effective averaging induced by the rotation of the detectors (see Fig. 7). It should be also noticed that, unlike the minimum value $G_{\Delta \min}(\gamma_{AA'}, \gamma_{EE'})$ in Eq. (43), we now keep the explicit K -dependence of the original ex-

pression $G_\Delta(K, \gamma_{AA'}, \gamma_{EE'})$ for the statistical gain. This allows us to see the cooperation of the noise ratio K and the ORFs $(\gamma_{AA'}, \gamma_{EE'})$ for the statistical gain.

In Fig. 10, we show our numerical results. We can observe a relatively small gain (e.g. $G_\Delta \lesssim 1.4$) only around the frequency regime $0.2\text{mHz} \lesssim f \lesssim 3\text{mHz}$ where the magnitude of the confusion noise becomes $K \gtrsim 1$. For the angle $\theta = 40^\circ$ currently designed for the LISA-Taiji network, we could have $G_\Delta \sim 1.65$ around $f \sim 0.4\text{mHz}$. If we take $80^\circ < \theta < 180^\circ$, the gain could be $G_\Delta \gtrsim 1.93$ in all the frequency range.

So far, we have assumed that the confusion noise level $N_B(f)$ is independent of the orbital configuration of the detector network (not only ignoring its dependence on the numbers of the units). But, in Fig. 10, the subtraction of the Galactic binaries is likely to work more efficiently at the regions with higher G_Δ . Then, the residual noise $N_B(f)$ itself would become smaller at the corresponding regions. Therefore, the actual contrast of the ratio σ_{2U}/σ_{1U} would be somewhat larger than Fig. 10.

V. SUMMARY AND DISCUSSION

In this paper, we studied performance of gravitational wave networks under the existence of coherent background noises. We introduced the effective number of detectors to characterize the statistical gain of the angular averaged sensitivity for a detector network.

We first examined the basic model for two L-shaped interferometers and derived the expression $G_2(K, \gamma)$ with the noise ratio K and the ORF γ . We discussed the overall properties of this expression, including its minimum value and the asymptotic profiles.

We then examined the effective number G_Δ for networks composed by two triangular detectors tangential to a sphere (see Eq. (41)). By using the symmetries of the systems, we could handle the problem as a straightforward extension of the basic model. The expression G_Δ can be applied not only to ground based detector networks but also to space detectors such as the LISA-Taiji network. The related expression (42) would be useful for a weak background level $K \ll 1$.

The magnitude of the noise ratio K cannot be securely measured beforehand for an essentially new frequency window. Therefore, as the worst case, we calculated the minimum value of the expression G_Δ , and discussed the preferable network geometry to suppress the potential reduction of the statistical gain. We can guarantee large gains $G_\Delta \gtrsim 1.9$ for the angular separation in the range $70^\circ < \beta < 105^\circ$, corresponding to the orbital phase difference $89^\circ < \theta < 153^\circ$ for space detectors (see Figs. 6 and 8).

Finally, under the approximation that the Galactic confusion background is isotropic, we examined its impacts on the two LISA-like units, by plugging in the estimated ratio K . With the currently proposed value $\theta = 40^\circ$ for the LISA-Taiji network, we have $G_\Delta \sim 1.65$

around 0.4mHz. By taking the orbital phase difference $\theta > 80^\circ$, we can increase the statistical gains to $G_\Delta \gtrsim 1.93$ in all the frequency range.

For suppressing the background noise correlation, our basic strategy was to reduce the absolute values of the ORFs. But, this is the opposite direction for enhancing the sensitivity to backgrounds by correlation analysis. It might be worth considering to take a balance between the two requirements.

In this paper, we have focused on the angular averaged sensitivity, as one of the fundamental quantities to characterize detector networks. But it would be interesting to examine impacts of the background noise correlation on other measures. Considering the active studies on the

space detector networks, it would be also meaningful to extend the present study to include anisotropies of the Galactic confusion background and make detailed studies on the preferable network geometry.

Acknowledgments

The author would like to thank H. Omiya for useful conversations. This work is supported by JSPS Kakenhi Grant-in-Aid for Scientific Research (Nos. 17H06358 and 19K03870).

-
- [1] B. P. Abbott *et al.* [LIGO Scientific and Virgo], Phys. Rev. Lett. **116**, no.6, 061102 (2016) doi:10.1103/PhysRevLett.116.061102 [arXiv:1602.03837 [gr-qc]].
- [2] B. P. Abbott *et al.* [LIGO Scientific and Virgo], Phys. Rev. X **9**, no.3, 031040 (2019) doi:10.1103/PhysRevX.9.031040 [arXiv:1811.12907 [astro-ph.HE]].
- [3] B. P. Abbott *et al.* [KAGRA, LIGO Scientific and VIRGO], Living Rev. Rel. **21**, no.1, 3 (2018) doi:10.1007/s41114-018-0012-9 [arXiv:1304.0670 [gr-qc]].
- [4] S. Hild, M. Abernathy, F. Acernese, P. Amaro-Seoane, N. Andersson, K. Arun, F. Barone, B. Barr, M. Barsuglia and M. Beker, *et al.* Class. Quant. Grav. **28**, 094013 (2011) doi:10.1088/0264-9381/28/9/094013 [arXiv:1012.0908 [gr-qc]].
- [5] D. Reitze, R. X. Adhikari, S. Ballmer, B. Barish, L. Barsotti, G. Billingsley, D. A. Brown, Y. Chen, D. Coyne and R. Eisenstein, *et al.* Bull. Am. Astron. Soc. **51**, no.7, 035 (2019) [arXiv:1907.04833 [astro-ph.IM]].
- [6] P. L. Bender *et al.*, LISA Pre-Phase A Report, Second edition, July 1998.
- [7] P. Amaro-Seoane *et al.* [arXiv:1702.00786 [astro-ph]].
- [8] J. Luo *et al.*, Class. Quant. Grav. **33**, no.3, 035010 (2016) doi:10.1088/0264-9381/33/3/035010 [arXiv:1512.02076 [astro-ph.IM]].
- [9] S. J. Huang, Y. M. Hu, V. Korol, P. C. Li, Z. C. Liang, Y. Lu, H. T. Wang, S. Yu and J. Mei, Phys. Rev. D **102**, no.6, 063021 (2020) doi:10.1103/PhysRevD.102.063021 [arXiv:2005.07889 [astro-ph.HE]].
- [10] W. R. Hu and Y. L. Wu, Natl. Sci. Rev. **4**, 685 (2017).
- [11] S. Kawamura, *et al.* [arXiv:2006.13545 [gr-qc]].
- [12] N. Christensen, Phys. Rev. D **46**, 5250-5266 (1992) doi:10.1103/PhysRevD.46.5250
- [13] E. E. Flanagan, Phys. Rev. D **48**, 2389 (1993).
- [14] B. Allen and J. D. Romano, Phys. Rev. D **59**, 102001 (1999).
- [15] J. D. Romano and N. J. Cornish, Living Rev. Rel. **20**, no.1, 2 (2017) doi:10.1007/s41114-017-0004-1 [arXiv:1608.06889 [gr-qc]].
- [16] B. P. Abbott *et al.* [LIGO Scientific and Virgo], Phys. Rev. D **100**, no.6, 061101 (2019) doi:10.1103/PhysRevD.100.061101 [arXiv:1903.02886 [gr-qc]].
- [17] C. Caprini and D. G. Figueroa, Class. Quant. Grav. **35**, no.16, 163001 (2018) doi:10.1088/1361-6382/aac608 [arXiv:1801.04268 [astro-ph.CO]].
- [18] T. Robson, N. J. Cornish and C. Liu, Class. Quant. Grav. **36**, no.10, 105011 (2019) doi:10.1088/1361-6382/ab1101 [arXiv:1803.01944 [astro-ph.HE]].
- [19] E. Thrane, N. Christensen and R. Schofield, Phys. Rev. D **87**, 123009 (2013) doi:10.1103/PhysRevD.87.123009 [arXiv:1303.2613 [astro-ph.IM]].
- [20] I. Kowalska-Leszczynska, M. A. Bizouard, T. Bulik, N. Christensen, M. Coughlin, M. Golkowski, J. Kubisz, A. Kulak, J. Mlynarczyk and F. Robinet, *et al.* Class. Quant. Grav. **34**, no.7, 074002 (2017) doi:10.1088/1361-6382/aa60eb [arXiv:1612.01102 [astro-ph.IM]].
- [21] Y. Himemoto and A. Taruya, Phys. Rev. D **100**, no.8, 082001 (2019) doi:10.1103/PhysRevD.100.082001 [arXiv:1908.10635 [astro-ph.IM]].
- [22] A. Matas and J. D. Romano, Phys. Rev. D **103**, no.6, 062003 (2021) doi:10.1103/PhysRevD.103.062003 [arXiv:2012.00907 [gr-qc]].
- [23] C. Cutler and E. E. Flanagan, Phys. Rev. D **49**, 2658-2697 (1994) doi:10.1103/PhysRevD.49.2658 [arXiv:gr-qc/9402014 [gr-qc]].
- [24] T. L. Smith, E. Pierpaoli and M. Kamionkowski, Phys. Rev. Lett. **97**, 021301 (2006) doi:10.1103/PhysRevLett.97.021301 [arXiv:astro-ph/0603144 [astro-ph]].
- [25] N. Seto, Phys. Rev. Lett. **125**, 251101 (2020) doi:10.1103/PhysRevLett.125.251101 [arXiv:2009.02928 [gr-qc]].
- [26] H. Omiya and N. Seto, Phys. Rev. D **102**, no.8, 084053 (2020) doi:10.1103/PhysRevD.102.084053 [arXiv:2010.00771 [gr-qc]].
- [27] T. A. Prince, M. Tinto, S. L. Larson and J. Armstrong, Phys. Rev. D **66**, 122002 (2002) doi:10.1103/PhysRevD.66.122002 [arXiv:gr-qc/0209039 [gr-qc]].
- [28] G. Mentasti and M. Peloso, JCAP **03**, 080 (2021) doi:10.1088/1475-7516/2021/03/080 [arXiv:2010.00486 [astro-ph.CO]].
- [29] G. Orlando, M. Pieroni and A. Ricciardone, JCAP **03**, 069 (2021) doi:10.1088/1475-7516/2021/03/069 [arXiv:2011.07059 [astro-ph.CO]].
- [30] G. Wang, W. T. Ni, W. B. Han, P. Xu and Z. Luo,

- [arXiv:2105.00746 [gr-qc]].
- [31] N. Seto, Phys. Rev. D **102**, no.12, 123547 (2020) doi:10.1103/PhysRevD.102.123547 [arXiv:2010.06877 [gr-qc]].
- [32] Z. C. Liang, Y. M. Hu, Y. Jiang, J. Cheng, J. d. Zhang and J. Mei, [arXiv:2107.08643 [astro-ph.CO]].
- [33] G. Wang and W. B. Han, [arXiv:2108.11151 [gr-qc]].
- [34] G. Giampieri and A. G. Polnarev, MNRAS **291**, 149 (1997).
- [35] C. Ungarelli and A. Vecchio, Phys. Rev. D **64**, 121501 (2001) doi:10.1103/PhysRevD.64.121501 [arXiv:astro-ph/0106538 [astro-ph]].
- [36] N. Seto, Phys. Rev. D **69**, 123005 (2004) doi:10.1103/PhysRevD.69.123005 [arXiv:gr-qc/0403014 [gr-qc]].
- [37] J. A. Edlund, M. Tinto, A. Krolak and G. Nelemans, Phys. Rev. D **71**, 122003 (2005) doi:10.1103/PhysRevD.71.122003 [arXiv:gr-qc/0504112 [gr-qc]].
- [38] T. Littenberg, N. Cornish, K. Lackeos and T. Robson, Phys. Rev. D **101**, no.12, 123021 (2020) doi:10.1103/PhysRevD.101.123021 [arXiv:2004.08464 [gr-qc]].